MARCH 22 2017

Vortex sound radiation in a flow duct with a dipole source and a flexible wall of finite length

Y. K. Chiang; Y. S. Choy; S. K. Tang

J. Acoust. Soc. Am. 141, 1999–2010 (2017)
https://doi.org/10.1121/1.4978521

Vortex sound radiation in a flow duct with a dipole source and a flexible wall of finite length

Y. K. Chiang,[1] Y. S. Choy,[1,a)] and S. K. Tang[2]
[1]*Department of Mechanical Engineering, The Hong Kong Polytechnic University, Hung Hom, Kowloon, Hong Kong Special Administrative Region, China*
[2]*Department of Building Services Engineering, The Hong Kong Polytechnic University, Hung Hom, Kowloon, Hong Kong Special Administrative Region, China*

(Received 9 May 2016; revised 8 February 2017; accepted 26 February 2017; published online 22 March 2017)

The noise attenuation of fan-ducted noise at low blade-passage frequency remains a challenge. The present study investigates the noise reduction mechanism of a tensioned membrane housing device that directly controls the sound radiation from the doublet which is enclosed in an infinitely long duct with a point vortex. The time dependent sound radiation mechanism and the vibro-acoustics coupling mechanism of the systems are studied by adopting the potential theory and matched asymptotic expansion technique. The silencing performance of such a passive approach depends on the amplitude and phase of the sound field created by the doublet and the acoustic pressure induced by the membrane oscillation in order to achieve sound cancellation. Results show that the response of membrane vibration is strongly associated with the flow field induced by the grazing uniform flow and also the fluid loading generated by the inviscid vortex. The geometrical property of the cavity and the mechanical properties of the flexible membranes play important roles in controlling the performance of the proposed device. © *2017 Acoustical Society of America*.
[http://dx.doi.org/10.1121/1.4978521]

[JDM] Pages: 1999–2010

I. INTRODUCTION

Ventilation systems are an essential component in modern commercial buildings as they effectively improve the comfort of human beings by circulating the air and delivering treated air to occupied zones within the building through ductwork from the air-handling unit. However, the noise from the air handling unit caused by the operation of fans continues to propagate to the work areas. The attenuation of the associated noise, including the tonal noise induced by the rotor and stator interaction and the broadband aerodynamic noise generated by vortex shedding and turbulence (Sharland, 1964; Longhouse, 1977), remains a technical challenge using passive noise control methods. Traditionally, duct lining (Ingard, 1995; Beranek and Vér, 2006) in which the porous material dissipates the noise by converting the acoustical energy into heat is commonly adopted in air conditioning systems. However, its performance is ineffective at low frequencies due to high impedance mismatch at the interface of air to traditional porous material. Apart from this, the environmental problem caused by the use of fibre material is also problematic (Fuchs, 2001a,b). On the other hand, a fibreless reactive silencing device, expansion chamber (Munjal, 1987), or multiple chambers (Ji, 2005) can be feasible solutions to control noise levels through the mechanism of sound reflection due to the change of cross-sectional area. However, these noise reduction mechanisms induce unavoidable pressure loss and thus increases the power consumption of the fans. In order to eliminate the pressure loss, active noise control was proposed to attenuate the tonal noise from a small axial flow fan (Wang *et al.*, 2005). Although it successfully provides tonal noise reduction, the requirement of sensors and actuators makes the system difficult to implement. Huang (1999) introduced the concept of a drum-like silencer, which is composed of two stretched light membranes covered with two side branch cavities. The prototype device has been examined successfully without flow (Huang *et al.*, 2000; Choy and Huang, 2002) and with mean flow (Choy and Huang, 2005). The harmonic responses of the membranes and the noise attenuation were analytically obtained in the frequency domain (Huang, 2002). However, the silencing performances predicted in the previous studies are limited for duct systems with uniform mean flow. The turbulent flow generated during fan operation has not been considered. When the fan is in operation, the flow generated is turbulent and hence the time-varying turbulent flow interacts with the flexible boundaries of the housing device in a more intricate vibro-acoustic mechanism. An analytical model of the turbulent boundary layer and the motion of the unsteady turbulence is complicated. Therefore, recent work by Ostoich *et al.* (2013) used a direct numerical simulation approach in order to investigate the coupled fluid-structural interactions between the turbulent boundary layer and the thin steel panel with a free-stream Mach number of 2.25. The fluid domain computed by the compressible Navier-Stokes equations and the structural solution calculated by the nonlinear, finite-strain finite element solver were coupled through matching nodes at the interface. Later, Zhang and Bodony (2016) extended the simulation database to study the detailed behavior in and around the honeycomb liner, to estimate the

a)Electronic mail: mmyschoy@polyu.edu.hk

discharge coefficient, and to predict the acoustic impedance of the liner in the presence of grazing laminar and turbulent boundary layers as well as the incident sound waves. Apart from the direct numerical simulation, Howe (2003) employed a vortex analogy as a semi-analytical approach which simply models the turbulent eddies as discrete point vortices. Tang *et al.* (2005) worked out the vortex motion, the far-field aeroacoustic radiation, and monopole sound pressure fluctuation induced by an oscillating flexible wall which interacts strongly with the inviscid vortex and grazing flow, where the cavity was not a consideration in the model. Afterwards, Tang (2011) studied the performance of a membrane covered by a cavity, which is the so-called drum-like silencer in the duct under low Mach number flow. However, he considered that acoustic pressure inside the cavity is distributed uniformly and is limited to a very shallow cavity. In fact, the corresponding height of the cavity would be one of the determinant factors in designing the silencing device as the flexible boundary vibration depends on the pressure loading acting on it.

On the other hand, fan noise can be controlled directly at the source itself. Recently, Liu *et al.* (2014) introduced a device consisting of two tensioned membranes backed with cavities housing the axial fan, which is the so-called membrane housing device for suppression of the sound radiation from the axial fan directly. This membrane house device can effectively suppress the low frequency noise analytically and experimentally. For realistic application in air conditioning systems such as air handling units with fan operation, where there are a number of aerodynamic noises created during fan operation. Regarding the aeroacoustics research for rotating machines, Gutin (1948) was the first to quantify the propeller noise caused by the rotation of steady loading that is called Gutin noise. The acoustic analogy of Lighthill (1952) contributed a formal platform to study aerodynamic sound. The first extension of Lighthill's theory was proposed by Curle (1955) who considered the effect of solid boundaries by replacing them with distributed dipoles. Afterwards, Ffowcs Williams and Hawkings (1969) formally extended the work of Lighthill by taking into account the effect of all solid boundaries in arbitrary motion. The solid surfaces act as "mirrors" of aerodynamics quadrupoles, giving rise to dipoles distributed over the solid surfaces. Generally speaking, there are three types of noise sources in any machine with moving blades: monopole from the blade motion, dipole from the fluctuating forces on blades, and quadrupole emanating from the core of turbulence jets. Focusing on the operation of axial fans at subsonic speed, it is found that the dominant noise source is often the unsteady pressure fluctuation arising from the interaction between the rotating blades and stationary blades. In the present study, the noise generated by the tip leakage flow and the turbulent layer on blade and rotor-stator interaction induced fluid loading fluctuation is characterized as a dipole source. The performance of using the membrane housing silencing device to control subsonic axial fan radiated tonal noise of a dipole nature directly at the source position was recently investigated by Liu *et al.* (2012) analytically with the mean flow condition simplified as steady uniform flow and validated by experiments. Previous work was conducted in a frequency domain in which the time-dependent excitation from the fan and response of membranes were neglected. The influence of flow turbulence and the corresponding to the unsteady flow sound generation mechanism were not presented.

A simplified theoretical aeroacoustic model of the membrane housing silencing device flush-mounted on the wall at the source location is established in the present study to gain insight into the flow-structure-acoustics interactions and aeroacoustics generation mechanism. The proposed theoretical model has the following distinct features. (a) It is different from the previous studies which mainly focused on the vortex-membrane interactions. A dipole sound source is considered, which leads to more complicated fluid-structural interactions. Moreover, the noise attenuation mechanism of the membrane housing device controlling the dipole source is studied with different designing parameters. (b) Inside the backed-cavity, a non-uniform fluid pressure is considered instead of assuming an even pressure distribution in order to simulate a more realistic transient response of the fully coupled membrane-cavity system. In order to examine the time varying fluid field corresponding to the dipole nature of fan noise, it is described as a doublet which is composed of two sources with anti-phase volume flow rate. The unsteady turbulent eddy is represented by an inviscid point vortex for simplification. In addition, a finite difference time domain (FDTD) approach (Kowalczyk and Van Walstijn, 2008) was adopted to explore the non-uniform fluid pressure distribution inside both the upper and lower cavities.

In what follows, Sec. II outlines a two-dimensional theoretical model and analytical formulation in details. The analysis of vortex dynamics and the noise radiation mechanism as well as the design parameters affecting the silencer performance are discussed in Sec. III. In Sec. IV, the main conclusions are summarized.

II. THEORETICAL MODELLING

Figure 1 shows the two-dimensional configuration of the silencing device, which is composed of two flush-mounted membranes of length L covering a side-branch rigid-walled cavity with depth h_c in an otherwise rigid-walled duct with a height a. The membranes are supported at both the leading ($x=-L/2$) and trailing edges ($x=L/2$), and the tension T is applied along the axial direction. A doublet is placed at the center of the silencing device. The doublet is composed of a source and a sink which have the same amplitude of strength μ_0 and operating frequency f at the small separation distance 2ε. The turbulent flow condition of high Reynolds number and low Mach number are considered in the present study so that the effect of viscosity can be ignored for simplicity (Katz and Plotkin, 2001). An inviscid vortex with circulation Γ is initially located at the x-coordinate x_e with the same axial position of doublet and at the y-coordinate y_e which depends on the length of the blades as it is practically shed at the trailing edge. The vortex propagates through the membrane and duct section under the effects of membranes vibration, doublet radiation, and the mean flow U. The instantaneous position of vortex is expressed as (x_v, y_v) in Sec. II A.

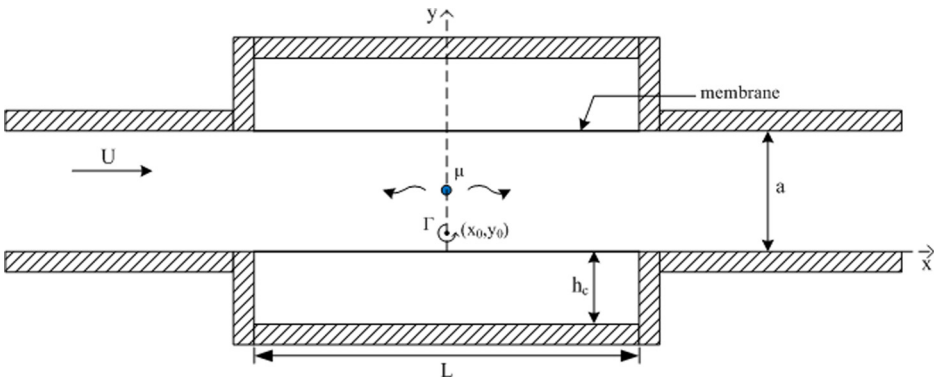

FIG. 1. (Color online) Two-dimensional configuration of the membrane housing device with a doublet.

A. Vortex dynamics and membrane vibrations

The dipole nature of the sound radiation in the fan-ducted system is modeled as a doublet inside a channel. The fluid velocity v_{dou} along the duct at any position (x, y) due to the influence of the doublet and its image, by utilizing the potential theory (Currie, 2013), is expressed as follows:

$$
\begin{aligned}
v_{dou}(x,y) = \hat{x}\frac{\mu}{2a}\Bigg\{ & e^{\pi(x_d-\varepsilon-x)/a}\Bigg[\frac{\cos\big(\pi(y-y_d)/a\big)-e^{\pi(x_d-\varepsilon-x)/a}}{e^{2\pi(x_d-\varepsilon-x)/a}-2e^{\pi(x_d-\varepsilon-x)/a}\cos\big(\pi(y-y_d)/a\big)+1} \\
& +\frac{\cos\big(\pi(y+y_d)/a\big)-e^{\pi(x_d-\varepsilon-x)/a}}{e^{2\pi(x_d-\varepsilon-x)/a}-2e^{\pi(x_d-\varepsilon-x)/a}\cos\big(\pi(y+y_d)/a\big)+1}\Bigg] - e^{\pi(x_d+\varepsilon-x)/a} \\
& \times\left[\frac{\cos\big(\pi(y-y_d)/a\big)-e^{\pi(x_d+\varepsilon-x)/a}}{e^{2\pi(x_d+\varepsilon-x)/a}-2e^{\pi(x_d+\varepsilon-x)/a}\cos\big(\pi(y-y_d)/a\big)+1}+\frac{\cos\big(\pi(y+y_d)/a\big)-e^{\pi(x_d+\varepsilon-x)/a}}{e^{2\pi(x_d+\varepsilon-x)/a}-2e^{\pi(x_d+\varepsilon-x)/a}\cos\big(\pi(y+y_d)/a\big)+1}\right]\Bigg\} \\
& +\hat{y}\frac{\mu}{2a}\Bigg\{ e^{\pi(x_d-\varepsilon-x)/a}\Bigg[\frac{\sin\big(\pi(y-y_d)/a\big)}{e^{2\pi(x_d-\varepsilon-x)/a}-2e^{\pi(x_d-\varepsilon-x)/a}\cos\big(\pi(y-y_d)/a\big)+1} \\
& +\frac{\sin\big(\pi(y+y_d)/a\big)}{e^{2\pi(x_d-\varepsilon-x)/a}-2e^{\pi(x_d-\varepsilon-x)/a}\cos\big(\pi(y+y_d)/a\big)+1}\Bigg] - e^{\pi(x_d+\varepsilon-x)/a} \\
& \times\left[\frac{\sin\big(\pi(y-y_d)/a\big)}{e^{2\pi(x_d+\varepsilon-x)/a}-2e^{\pi(x_d+\varepsilon-x)/a}\cos\big(\pi(y-y_d)/a\big)+1}+\frac{\sin\big(\pi(y+y_d)/a\big)}{e^{2\pi(x_d+\varepsilon-x)/a}-2e^{\pi(x_d+\varepsilon-x)/a}\cos\big(\pi(y+y_d)/a\big)+1}\right]\Bigg\},
\end{aligned}
\tag{1}
$$

where μ is the rate of volume flow issuing outward (inward) from the source (sink) (Vallentine, 1959), which is expressed as a harmonic form, i.e., $\mu(\tau)=\mu_0\cos(2\pi f\tau)$, (x_d, y_d) is the location of the doublet, τ represents time, a is the height of duct, and $\hat{x}$ and $\hat{y}$ are the unit vector. Note that the position of doublet is taken as the middle point between the source and the sink.

The membranes are initially at rest, it is then subjected into motion due to the excitation by grazing mean flow, vortex acceleration and also the doublet radiation. For small membrane vibration magnitudes, the vibrating membranes are modeled as rigid boundaries with distributed fluctuating normal velocities presented by Tang (2011). The fluid velocity, v_{mem}, at any position (x, y) inside a duct due to the flow induced by membranes vibration is estimated by an integration along the membranes. The detail expression of the induced velocity due to the membrane vibration have been given by Tang (2011).

When the blade starts its motion impulsive from $\tau=0$, there is a starting vortex with circulation $\Gamma(\tau)$ due to flow separation at the sharp trailing edge of the blade. The growth of the vortex strength is determined by the Kutta condition. It is related to the chord-line of blade c, the angle of attack α, and also the uniform speed is far-field U_∞. The general expression of the circulation is $\Gamma(\tau)=2U\alpha(cU\tau)^{0.5}$. When $\tau \to \infty$, the limiting circulation would be $\Gamma_\infty=\pi c\alpha U_\infty$ (Saffman, 1992). According to Brown and Michael (1954), the vortex velocity including its self-induced velocity is written as

$$
\begin{aligned}
v_{vortex}(x_v,y_v) = & \hat{x}\left[-\frac{x_v-x_e}{\Gamma}\frac{d\Gamma}{d\tau}+U+\frac{\Gamma}{4a}\cot\frac{\pi y_v}{a}\right] \\
& +\hat{y}\left[-\frac{y_v-y_e}{\Gamma}\frac{d\Gamma}{d\tau}\right]+v_{mem}(x_v,y_v) \\
& +v_{dou}(x_v,y_v).
\end{aligned}
\tag{2}
$$

The instantaneous vortex motion, harmonic radiation of doublet and mean flow give rise to fluctuating pressure loading on the two membranes. The response of membranes are governed by

$$m\frac{\partial^2\eta_l}{\partial\tau^2}-T\frac{\partial^2\eta_l}{\partial x'^2}+D\frac{\partial\eta_l}{\partial\tau}+(p_{l,duct}-p_{l,cavity})=0$$

and

$$m\frac{\partial^2\eta_u}{\partial\tau^2}-T\frac{\partial^2\eta_u}{\partial x'^2}+D\frac{\partial\eta_u}{\partial\tau}+(p_{u,cavity}-p_{u,duct})=0, \tag{3}$$

where p is the fluid pressure and the subscript "duct" and "cavity" represent the meaning of the duct section and cavity section, respectively. m is the mass density of the membrane, T is the tension applied on the membrane per unit length, and D represents the damping coefficient.

The duct-side pressure loading which exists on the surface of membranes can be obtained by the linearized Bernoulli equations (Peake, 2004)

$$p_{l,duct}=-\rho_0\left(\frac{\partial\phi}{\partial\tau}+U\frac{\partial\phi}{\partial x}\right)\Big|_{y=\eta_l}$$

and

$$p_{u,duct}=-\rho_0\left(\frac{\partial\phi}{\partial\tau}+U\frac{\partial\phi}{\partial x}\right)\Big|_{y=\eta_u},$$

where ρ_0 is the fluid density and ϕ is the velocity potential in the duct. The total incompressible velocity potential in near-field at any position (x, y) in the channel is generally written as

$$\begin{aligned}\phi(x,y,\tau)=&-\frac{\Gamma}{2\pi}\tan^{-1}\left[\frac{2\sin(\pi y_v/a)\left(e^{\pi(x-x_v)/a}\cos(\pi y/a)-\cos(\pi y_v/a)\right)}{\left(e^{\pi(x-x_v)/a}\cos(\pi y/a)-\cos(\pi y_v/a)\right)^2+\left(e^{\pi(x-x_v)/a}\sin(\pi y/a)\right)^2-(\sin(\pi y_v/a))^2}\right]\\&+\frac{1}{2\pi}\int_{-L/2}^{L/2}\left(\frac{\partial\eta_l}{\partial\tau}+U\frac{\partial\eta_l}{\partial x'}\right)\log\left[\cosh\left(\pi(x-x')/a\right)-\cos\left(\pi(y-\eta_l)/a\right)\right]dx'\\&-\frac{1}{2\pi}\int_{-L/2}^{L/2}\left(\frac{\partial\eta_u}{\partial\tau}+U\frac{\partial\eta_u}{\partial x'}\right)\log\left[\cosh\left(\pi(x-x')/a\right)+\cos\left(\pi(y-\eta_u)/a\right)\right]dx'\\&+\frac{\mu(\tau)}{4\pi}\log\left[\frac{e^{2\pi(x_d-\varepsilon-x)/a}-2e^{\pi(x_d-\varepsilon-x)/a}\cos\left(\pi(y_d-y)/a\right)+1}{e^{2\pi(x_d+\varepsilon-x)/a}-2e^{\pi(x_d+\varepsilon-x)/a}\cos\left(\pi(y_d-y)/a\right)+1}\right]\\&+\frac{\mu(\tau)}{4\pi}\log\left[\frac{e^{2\pi(x_d-\varepsilon-x)/a}-2e^{\pi(x_d-\varepsilon-x)/a}\cos\left(\pi(y_d+y)/a\right)+1}{e^{2\pi(x_d+\varepsilon-x)/a}-2e^{\pi(x_d+\varepsilon-x)/a}\cos\left(\pi(y_d+y)/a\right)+1}\right]+Ux+\gamma(\tau),\end{aligned} \tag{4}$$

where γ is a time function. The expression can be deduced by using the matched asymptotic expansion described in Sec. II B. On the right-hand-side of Eq. (4), the first term is the flow potentials induced by vortex and its images with the use of method of infinite images (Vallentine, 1959). The second and third terms describe the potentials corresponding to the membranes oscillations. The contribution of radiations of the doublet and its images is expressed as the fourth and fifth terms, respectively.

The flexible membranes are backed by the cavity with the same length of the membrane as illustrated in Fig. 1. It is a fully coupled membrane-cavity system. The vibration of flexible membrane induces acoustic pressure fluctuation inside the cavity. The pressure loading induced inside the cavity acts on the membrane and hence affects the membrane vibration. The pressure distribution in the cavity can be estimated by the FDTD method with the conservation of momentum and the continuity equation. The longitudinal and transverse particle velocities, denoted as v_x and v_y, are obtained by discretizing the governing equations. The two-dimensional basic formulations of FDTD are

$$v_x^{n+0.5}\left(i+\frac{1}{2},j\right)=v_x^{n-0.5}\left(i+\frac{1}{2},j\right)-\frac{\Delta\tau}{\rho_0\Delta x}\times\left[p_{cavity}^n(i+1,j)-p_{cavity}^n(i,j)\right] \tag{5}$$

and

$$v_y^{n+0.5}\left(i,j+\frac{1}{2}\right)=v_y^{n-0.5}\left(i,j+\frac{1}{2}\right)-\frac{\Delta\tau}{\rho_0\Delta y}\times\left[p_{cavity}^n(i,j+1)-p_{cavity}^n(i,j)\right], \tag{6}$$

where $\Delta\tau$ is the temporal step size and Δx and Δy are the spatial size for x- and y-directions, respectively. The step sizes $\Delta\tau$, Δx, and Δy must be chosen to satisfy the Courant stability criterion $c_0\Delta\tau\le(1/\Delta x+1/\Delta y)^{-1/2}$ for the two-dimensional case (Taflove and Brodwin, 1975). Integers n indicate the time instant and i and j denote the spatial points along the x- and y-axes, respectively. The approximations of acoustic pressure at any point inside the cavity p_{cavity} are obtained by the discretized continuity equation

$$\begin{aligned}p_{cavity}^{n+1}(i,j)=&\,p_{cavity}^n(i,j)-\frac{\rho_0c_0^2\Delta\tau}{\Delta x}\left[v_x^{n+0.5}\left(i+\frac{1}{2},j\right)-v_x^{n+0.5}\left(i-\frac{1}{2},j\right)\right]\\&-\frac{\rho_0c_0^2\Delta\tau}{\Delta y}\times\left[v_y^{n+0.5}\left(i,j+\frac{1}{2}\right)-v_y^{n+0.5}\left(i,j-\frac{1}{2}\right)\right],\end{aligned} \tag{7}$$

where c_0 is the speed of sound. Apart from the oscillating flexible membrane, other three boundaries are rigid walls, which are treated as locally reacting surface, with frequency independent boundary conditions

$$\frac{\partial p_{cavity}}{\partial \tau} = -c_0 \xi_x \frac{\partial p_{cavity}}{\partial x} \quad \text{for } x = -L/2 \text{ and } x = L/2,$$

$$\frac{\partial p_{cavity}}{\partial \tau} = -c_0 \xi_y \frac{\partial p_{cavity}}{\partial y} \quad \text{for } y = -h_c \text{ and } y = a + h_c,$$

where ξ_x and ξ_y are the normalized impedances in the x- and y-directions, respectively. The pressure distribution inside the backed-cavity with different wall impedances can also be solved by modifying ξ_x and ξ_y (Kowalczyk and Van Walstijn, 2008). The membranes are initially regarded as stationary. The vortex accelerates, circulation grows, and membrane vibration starts with $\tau = 0$. The movement of vortex and the motion of membrane vibration can be predicted by time integration of Eqs. (1)–(11) with the use of the fourth order Runge-Kutta procedure. The motion of the vortex solved by the Runge-Kutta scheme can be written as

$$\begin{aligned}
K_1 &= v_{vortex}(Z_\tau, \tau),\\
K_2 &= v_{vortex}(Z_\tau + K_1 \times \Delta\tau/2, \tau + \Delta\tau/2),\\
K_3 &= v_{vortex}(Z_\tau + K_2 \times \Delta\tau/2, \tau + \Delta\tau/2),\\
K_4 &= v_{vortex}(Z_\tau + K_3 \times \Delta\tau, \tau + \Delta\tau),\\
Z_{\tau+\Delta\tau} &= Z_\tau + \frac{\Delta\tau}{6}(K_1 + 2K_2 + 2K_3 + K_4),
\end{aligned}$$

where $Z = (x_v, y_v)$.

B. Far-field acoustic radiation

The solution of far-field acoustic pressure radiation in the duct can be found using the matched asymptotic expansion which matches the inner region incompressible near-field solution to the outer region of the plane wave solution (Tang, 2011). The far-field plane wave equation with steady mean flow of low Mach number is (Howe, 1998)

$$(1 - M^2)\frac{\partial^2 \phi}{\partial x^2} - \frac{2M}{c_0}\frac{\partial^2 \phi}{\partial x \partial t} - \frac{1}{c_0^2}\frac{\partial^2 \phi}{\partial t^2} = 0,$$

where t is time in the far-field and M is the Mach number, i.e., $M = U/c_0$. The general solution, Φ, after the time-Fourier transformation is

$$\begin{aligned}
\Phi = {} & A_- \exp\left[i\omega x/(c_0(1 - M))\right]\\
& + A_+ \exp\left[-i\omega x/(c_0(1 + M))\right],
\end{aligned} \tag{8}$$

where A_- and A_+ are the complex magnitude of upstream going wave and downstream going wave, respectively, and ω is the angular frequency. The downstream approximated velocity potential far from the device, i.e., $x \to +\infty$ from Eq. (4), is

$$\begin{aligned}
\phi_{+\infty} \approx {} & -\frac{\Gamma}{\pi}\left(\frac{\pi y_v}{a}\right)e^{-\pi x/a}\\
& + \frac{x}{2a}\int_{-L/2}^{L/2}\left(\frac{\partial \eta_l}{\partial \tau} - \frac{\partial \eta_u}{\partial \tau}\right)dx' + \frac{2\varepsilon\mu}{a} + Ux + \gamma.
\end{aligned} \tag{9}$$

Since all of the waves propagate towards the downstream without moving reversely back to the near-field, the magnitude of upstream going wave in Eq. (8) is zero, i.e., $A_- = 0$. By the method of match asymptotic expansion, the asymptotic solution can be found for very low frequency, i.e., $\omega x/c_0 \to 0$, and very low Mach number, where $M \to 0$ (Sabina and Willis, 1975; Sabina and Babich, 2001). The leading order of the far-field solution suggests the sole function to be

$$\gamma(\tau) = \frac{c}{2a}\int_{-L/2}^{L/2}(\eta_u - \eta_l)dx'. \tag{10}$$

Hence, the complex magnitude A_+ can be obtained by applying Fourier transformation to the solution of fluid potential in far-field which is shown as

$$\phi_{far,+\infty} \approx -\frac{\Gamma y_v}{a} + \frac{2\varepsilon\mu}{a} + \frac{c}{2a}\int_{-L/2}^{L/2}(\eta_u - \eta_l)dx'.$$

The resultant acoustic pressure radiation far in downstream is

$$\begin{aligned}
p_{+\infty} &= -\rho_0\left(\frac{\partial \phi_{far,+\infty}}{\partial t} + U\frac{\partial \phi_{far,+\infty}}{\partial x}\right)\\
&= -\frac{\rho_0}{1 + M}\left[-\frac{\partial}{\partial \tau}\left(\frac{\Gamma y_v}{a}\right) + \frac{2\varepsilon}{a}\frac{\partial \mu}{\partial \tau}\right.\\
&\quad \left. + \frac{c_0}{2a}\int_{-L/2}^{L/2}\frac{\partial}{\partial \tau}(\eta_u - \eta_l)dx'\right],
\end{aligned} \tag{11}$$

which is evaluated at the retarded time $t - x/[c(1 + M)]$. The first term in the bracket is the sound radiation induced by the evolution of vortex circulation and the vortex velocity. The second term is the acoustic pressure radiated by the doublet induced force acting on the fluid. The sound wave generated by the volumetric flow excited by membranes vibration is expressed as the last term. Following similar procedures, as there is no wave moving back toward the near field form upstream, i.e., $A_+ = 0$, the low frequency acoustic wave radiation in upstream is given as

$$\begin{aligned}
p_{-\infty} &= -\rho_0\left(\frac{\partial \phi_{far,-\infty}}{\partial t} + U\frac{\partial \phi_{far,-\infty}}{\partial x}\right)\\
&= -\frac{\rho_0}{1 - M}\left[\frac{\partial}{\partial \tau}\left(\frac{\Gamma y_v}{a}\right) - \frac{2\varepsilon}{a}\frac{\partial \mu}{\partial \tau}\right.\\
&\quad \left. + \frac{c_0}{2a}\int_{-L/2}^{L/2}\frac{\partial}{\partial \tau}(\eta_u - \eta_l)dx'\right],
\end{aligned} \tag{12}$$

with retarded time $t + x/[c(1 - M)]$.

In the current study, the silencing performance of the membrane housing device is indicated by an insertion loss (IL) which is shown as

$$\mathrm{IL} = 10\log_{10}\frac{W_{original}}{W_{silenced}}, \tag{13}$$

where "original" refers to the unsilenced system and "silenced" refers to the silenced system with the membrane housing device. The acoustic power radiated, W, is obtained by integrating ${p_{rms}}^2/\rho_0 c_0$ over the cross section area of duct.

III. RESULTS AND DISCUSSION

In the present study, all variables are normalized by the duct height a^*, the fluid density ρ_0^*, and the maximum mean flow speed U_{max}^* chosen for the foregoing discussion with low Mach number conditions. The speed of the grazing uniform flow is ranged from zero to 50 m/s such that the current study is restricted in the subsonic regime. Three major mechanical properties of the membrane including the mass density m^*, the applied tension on the membrane per unit length T^*, and the damping coefficient D^* are normalized by $a^*\rho_0^*$, $U_{max}^*\rho_0^*$, and $a^*(U_{max}^*)^2\rho_0^*$, respectively. The damping coefficient is assigned as the same value as Tang (2011), i.e., $D^* = (\rho_0^* c_0^* a^*)$, for very weak damping condition (Frendi *et al.*, 1994). The center of the membrane is located at $x = 0$ and the total length is $L = 2$. The circulation of vortex remains $\Gamma_\infty = 2.74 \times 10^{-3}$ which has been normalized by $a^*U_{max}^*$. The initial coordinate of vortex is $x_e = 0$ and $y_e = 0.1$. Since the doublet is not movable, the position of doublet is fixed at (0, 0.5) in the present study with time dependent strength $\mu = \mu_0\cos(2\pi f\tau)$, where μ_0 is the amplitude of the volume flow rate per unit length that has been normalized by $a^*U_{max}^*$. The spatial sizes of the cavity are $\Delta x = \Delta y = 0.02$ and the time step $\Delta\tau$ is chosen as 0.001 such that the Courant stability condition is satisfied.

A. Flow-structural interactions

Figure 2 illustrates the effect of cavity depth of the silencing device and mass density of membrane on the vortex trajectories in the duct for the speed of grazing flow $U = 0.2$. The doublet has the strength $\mu_0 = 6$ and frequency $f = 0.68$. The vortex initially started its motion at $y_v = 0.1$. Figure 2(a) shows the vortex path at different cavity height for membrane property $m = 50$ and $T = 20$. Generally speaking, the vortex path eventually bends upward as the cavity height is increased. For the relatively shallow cavity $h_c = 0.5$ (solid lines), the upward motion of the vortex is less significant when comparing with the cases of having deeper backing cavity. In addition, the vortex is bended upward and resumes close to its original height shortly after for a shallower cavity such as $h_c = 0.5$. It seems that the vortex is propagating to the downstream of the duct with upward and downward movement under certain frequency. As stated by the previous study of Tang, the motion of vortex is strongly influenced by the membranes vibration which is fully coupled with the fluid pressure inside the duct and cavity. The change of cavity depth affects the compressibility of trapped

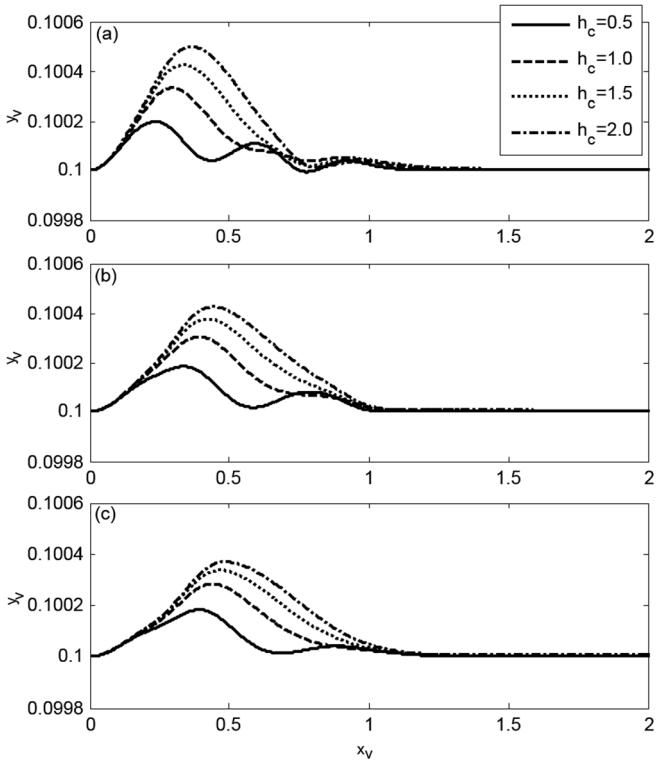

FIG. 2. Effects of cavity height and mass ratio on the vortex dynamics ($f = 0.68$, $\mu_0 = 6$, $U = 0.2$, $T = 20$, $y_e = 0.1$) for (a) $m = 50$, (b) $m = 100$, (c) $m = 150$.

air inside the cavity and thus, causes different membrane motion (Dowell and Voss, 1963). The details describing the corresponding vibration of membrane will be discussed later.

With increasing the mass density of the membrane, the similar trend of the vortex path is obtained as shown in Figs. 2(b) and 2(c). However, the magnitude of maximum variation of the vortex height slightly decreases with increasing membrane mass. It is observed that the maximum deviation of vortex height is 0.5% for $h_c = 2$ and $m = 50$. The deviation is slightly reduced to 0.42% and 0.37% for $m = 100$ and $m = 150$, respectively. Apart from it, the corresponding peak position of the vortex is shifted axially to the trailing edge of the membrane section when the mass of the membrane is increased. The same observation is found when a larger uniform flow speed $U = 1.0$ is considered in the duct. The maximum deviation of vortex height for $h_c = 2$ reduces from about 2.9% to around 1.3% when the mass density of membrane increases from 50 to 150.

Figure 3 shows the corresponding displacement and velocity along the lower membrane which influences the vortex movement as described in Fig. 2(a) with cavity height $h_c = 0.5$ (solid line) and $h_c = 1.0$ (dashed line) at different time instants. Three instantaneous locations of the vortex and the corresponding time are chosen. The circle and cross marked on the lines indicate the longitudinal position of the vortex at that specific time. Figures 3(1a) and 3(2a) show the vibration shape and the transverse velocity along the lower membrane, respectively, at $\tau = 0.498$. This shows that the phase at different positions of the membrane vibration is the

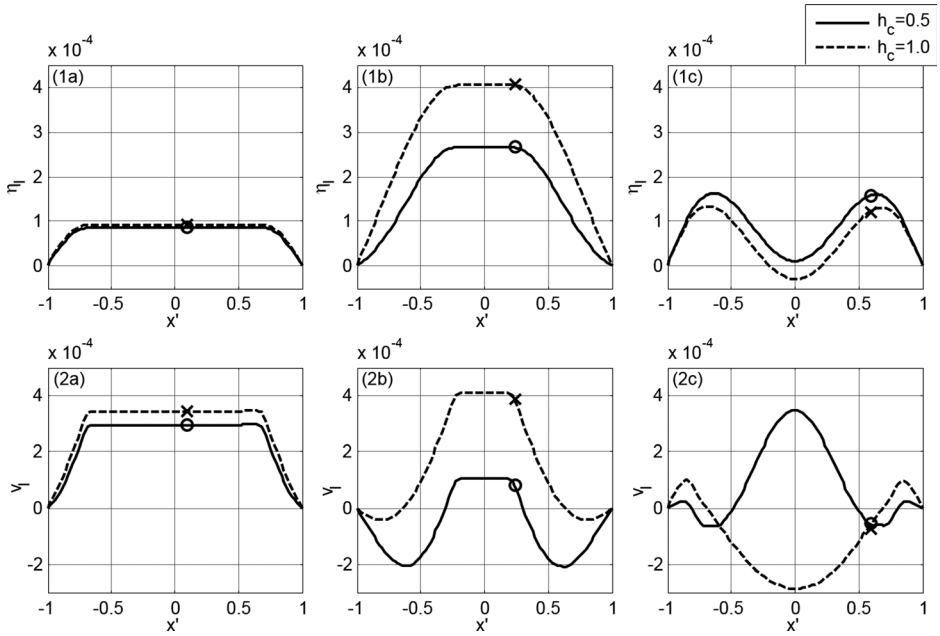

FIG. 3. Vibration shape of lower membrane. The first row represents the variation of displacement while the second row represents the velocity at (a) $\tau = 0.498$, (b) $\tau = 1.239$, (c) $\tau = 2.971$.

same for different cavity heights at the beginning when x_v is close to 0.1. The magnitude of the membrane vibration is slightly higher for larger cavity heights. Figures 3(1b) and 3(2b) show the response of the membrane at $\tau = 1.239$. When the cavity height is 1.0, the vortex reaches the peak position at $\tau = 1.23$ that is consistent with the motion of the membrane. When the cavity is shallower $h_c = 0.5$, the transverse velocity of the vortex is slower due to the weak response of the membrane covered by the shallow cavity. However, the vortex height is not always at higher levels for a deeper cavity. Figure 3(2c) shows the velocity of the membrane at $\tau = 2.971$. At this moment, the vortex reaches the longitudinal position $x = 0.6$ and the corresponding vortex height for $h_c = 0.5$ is higher than when $h_c = 1.0$. This observation can also be explained by the membrane motion. As shown in Fig. 3(1c), for $h_c = 0.5$, the membrane has a larger upward displacement when the vortex flies over at $x = 0.6$, resulting in an increase of vortex height. It is believed that the vortex motion depends critically on the phases of the membrane vibration at the instant the vortex interacts with the membrane.

Figures 4(1a)–4(1c) show the time history of the modal response of lower membrane with mass density $m = 50$, $m = 100$, and $m = 150$, respectively. The membrane responses are obtained by solving the motion governing equations as shown in Eq. (3). The first, second, and third modal response are represented by solid, dotted, and dashed lines, respectively. It is found that the oscillation of the membrane is dominant at odd modes while the second mode of vibration is less significant for different mass densities of the membrane. With the same excitation by the doublet and grazing flow at $U = 0.2$, the maximum amplitude of the

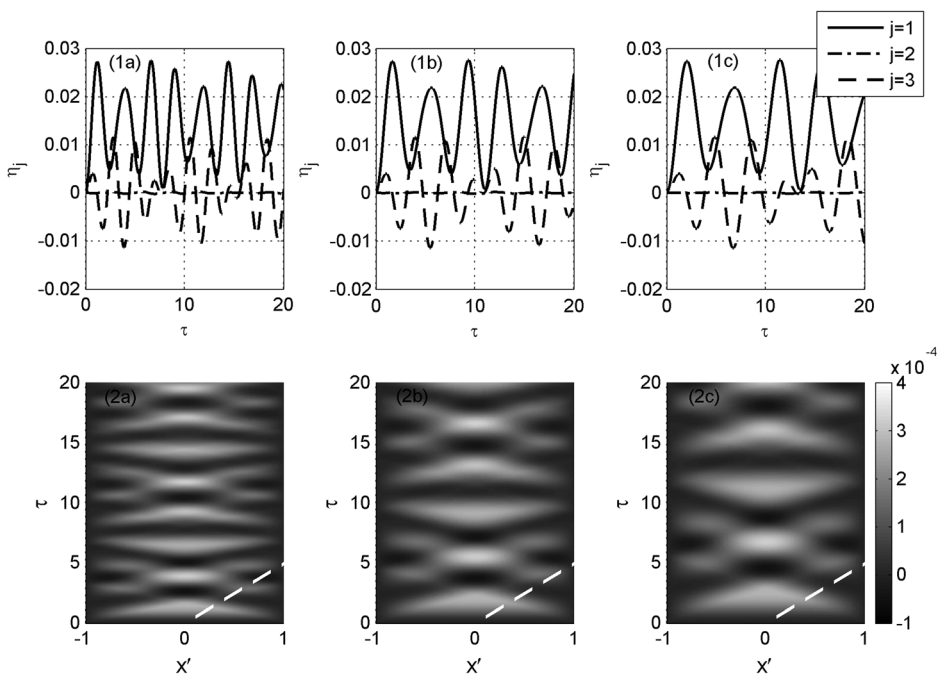

FIG. 4. Vibration displacement of lower membrane for $h_c = 0.5$. The first row represents the modal magnitude while the second row represents the time variation of vibration displacement of lower membrane of (a) $m = 50$, (b) $m = 100$, (c) $m = 150$.

membrane response is nearly the same for different mass densities of the membranes, but their oscillating frequencies are not the same. The *in vacuo* wave speed along the membrane, $c_T = (T/m)^{0.5}$, will be higher for lighter membranes. Hence the membranes oscillate at higher frequency when they respond to the same excitation of fluid loading. Figures 4(2a)–4(2c) depict the contour of the displacements of the lower membrane as a function of time τ and axial position x' for $m = 50$, 100, and 150, respectively. The dashed line represents the longitudinal position of the vortex x_e at the corresponding time. As previously discussed, the odd modes are dominant in the membrane vibration such that the maximum amplitude of displacement is always reached at the center of the membrane. Since the shed vortex has the initial x-position $x_e = 0$, which is also the center of the membrane, it has a higher chance to gain a larger transverse velocity caused by membrane vibration if the membrane could reach its vibration amplitude within a shorter time before the vortex is swept to the downstream of the silencer due to the mean flow.

With a shorter chord length of blade, the shed vortex evolved at the trailing edge of the fan blade is assumed to have a higher initial height. Figure 5 shows the relative transverse velocity of the vortex along the axial direction for different initial heights of vortex y_e, which is indicted in Eq. (2), when the membrane has $m = 100$, $T = 20$ with the cavity of $h_c = 0.8$ at $U = 0.1$. Tang showed that the increase of the initial height of the shed vortex weakens the interaction between the inviscid vortex and the lower membrane vibration. However, unlike the case of Tang, as shown in Fig. 5, the vortex transverse velocity is not weakened by the pressure-releasing effect of the upper membrane when a doublet is introduced to the duct. Figures 5(a) to 5(c) show variation of the relative vortex path at $f = 0.68$ for the strength of a doublet $\mu_0 = 3$, 6, and 9, respectively. Roughly speaking, the variation of the vortex height is increased with the strength of the doublet. Therefore, the instantaneous position of the vortex is not only influenced by the membrane vibration, but also the potential of the doublet radiation. In addition, there is a periodic fluctuation of the vortex height when the vortex initial height is increased or closed to the doublet position. As shown in Fig. 5(b), an even more significant vortex transverse velocity can be found by introducing a stronger doublet, i.e., $\mu_0 = 6$, when the vortex is initially shedded at a higher location. From the dotted lines in Figs. 5(a)–5(c), the vortex reaches its first peak at $\tau \sim 0.76$ and the second peak at $\tau \sim 2.20$. The results show that the oscillating frequency of the vortex path is around 0.69, which is close to the radiation frequency of the doublet. It is believed that the interaction between the pressure loading released by the doublet and the vortex dynamics becomes more dominant when initial vortex height is increased. However, the significance of the doublet effect vanishes when the vortex continuously propagates towards the trailing edge of the membrane. The flight paths of vortex are predicted with a similar shape when $x_v > 0.5$ for the cases of $y_e = 0.1$, 0.2, and 0.3, which is associated with the membrane motion instead of the fluid potential of doublet.

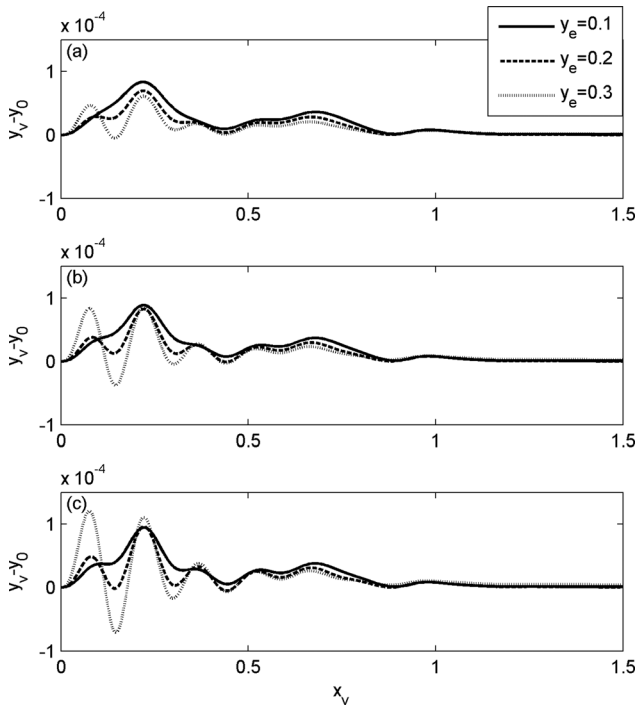

FIG. 5. Effect of doublet strength and initial vortex height on the vortex path for $h_c = 0.8$. (a) $\mu_0 = 3$, (b) $\mu_0 = 6$, (c) $\mu_0 = 9$.

B. Far-field acoustic pressure radiations

In order to further investigate the constituent of the sound pressure radiation to the downstream of the duct, the contributions from each noise source are examined in this section. The average sound pressure radiation from vortex with the strength $\Gamma_\infty = 0.00274$ is about one tenth of the total sound pressure radiation, which is significantly less than that of doublet and membrane. Hence the acoustic contribution from the vortex is not considered here. Figure 6 shows the sound pressure radiation generated by the doublet and membrane with different depth of backing cavity for $m = 100$, $T = 20$, $f = 0.68$, and $\mu_0 = 6$. The far-field acoustic radiations of the doublet and membrane shown as the last two terms of Eq. (11) are expressed as root mean square value. Generally, the sound radiation from the membrane is increased with the increasing of mean flow speed since the flow causes the change of the source strength of the acoustic field by the term $U\partial\phi_{far,+\infty}/\partial x$ in Eq. (11). Also, as shown by Sucheendran *et al.* (2013), the acoustic-structural coupling is more significant at higher flow speed, thus the acoustic response of the membrane vibration increases with Mach number. The cavity effect on the resultant sound radiation due to the membrane vibration which depends on the Mach number can be classified into three regions: region I is the zone with very small Mach number with $0.006 < M < 0.013$, region II is the intermediate zone for $0.013 \leq M \leq 0.018$, and region III is the zone with $M > 0.018$. In region I, the root mean square value of the sound pressure induced by the membrane, $p_{rms,m}$, is relatively small compared to a doublet, $p_{rms,d}$. The effect of cavity depth on the acoustic pressure radiation slightly increases with the Mach number. Since the excitation on the membrane caused by the grazing uniform flow is small, the induced pressure loading inside the cavity

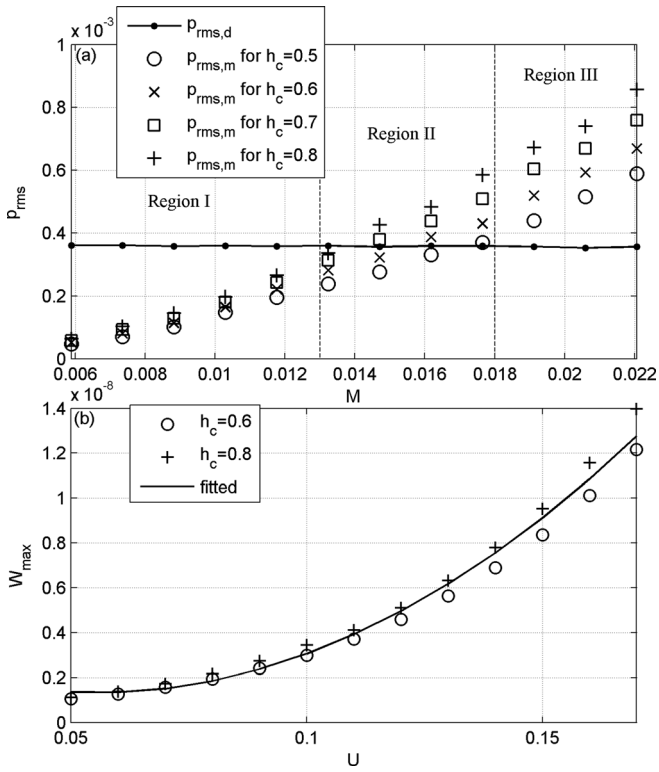

FIG. 6. Effect of mean flow speed on the sound radiation of membranes. (a) Root mean square value of acoustic pressure radiation; (b) Maximum sound power radiation. ($\mu_0 = 6, f = 0.68, U = 0.1, m = 100, T = 20, y_e = 0.1$).

is relatively small and thus the effect of cavity depth on the amplitude of sound pressure is not significant in this case. When the Mach number is increased to that of region II, the sound generated by the membrane is comparable with that generated by the fluid force from the doublet, $p_{rms,d}$. The influence of cavity height on the sound pressure radiation from the membrane becomes more crucial in this intermediate range. More than 41% sound radiation enhancement is found for the cavity height increased from $h_c = 0.5$ to 0.8 at M = 0.01324. Moreover, Fig. 6(a) shows that if the Mach number is further increased reaching region III, the membrane is then driven into a vigorous vibration such that sound would be amplified even for a different design of backed-cavity in this situation. Therefore, a better silencing performance could be achieved in regions I and II with low Mach number. The noise control mechanism with different design of the silencing device will be discussed in Sec. III C.

Figure 6(b) shows the maximum value of total sound power W_{max} radiated to the downstream of the duct as a function of flow speed. The acoustic power radiation is higher for larger cavity depth h_c at any mean flow speed. The maximum of sound power W_{max} increases with the mean flow speed nonlinearly. The same observation can be also found from region III illustrate in Fig. 6(a). The maximum sound power is possible to be expressed as the function of the grazing flow speed by a quadratic function in a normalized form

$$W_{\max} = (834.5U^2 - 92.28U + 3.848) \times 10^{-9}, \qquad (14)$$

for the case $m = 100, T = 20, f = 0.68$, and $\mu_0 = 6$.

C. Noise attenuation

The noise attenuation can be achieved by using the proposed membrane housing device based on the sound cancellation mechanism. The membranes are driven into vibration to generate sound which is accordingly superimposed with the aerodynamic noise and the dipole sound. Therefore, the amplitude and frequency of sound waves radiated by the cavity-backed membrane vibration are fairly important in determining the performance of such passive noise silencing devices. The designing parameters that affect the membrane motion shown in Eq. (3), including the geometric feature specified as the cavity depth and the mechanical properties of the flexible membrane such as the mass density and applied tension, would cause a change of the frequency and the amplitude of sound radiated by the membrane vibration and result in a different performance of the silencing device (Kim *et al.*, 2016). This will be discussed briefly in the following. The numerical results are obtained with three different mean flow speeds, $U = 0.05$, 0.1, and 0.2.

Figure 7 shows the sound pressure radiated by the doublet p_{dou} (dotted line), and that induced by the membrane vibration p_{mem} for three different cavity heights $h_c = 0.4$ (solid line), 0.6 (dashed line), and 0.8 (dash-dot line) with $f = 0.34$, $\mu_0 = 8$, $m = 90$, and $T = 40$. From Fig. 7(a), it is observed that the oscillation frequency of acoustic pressure radiation from the membrane becomes lower with increasing cavity height. When the shallow cavity is adopted, the cavity

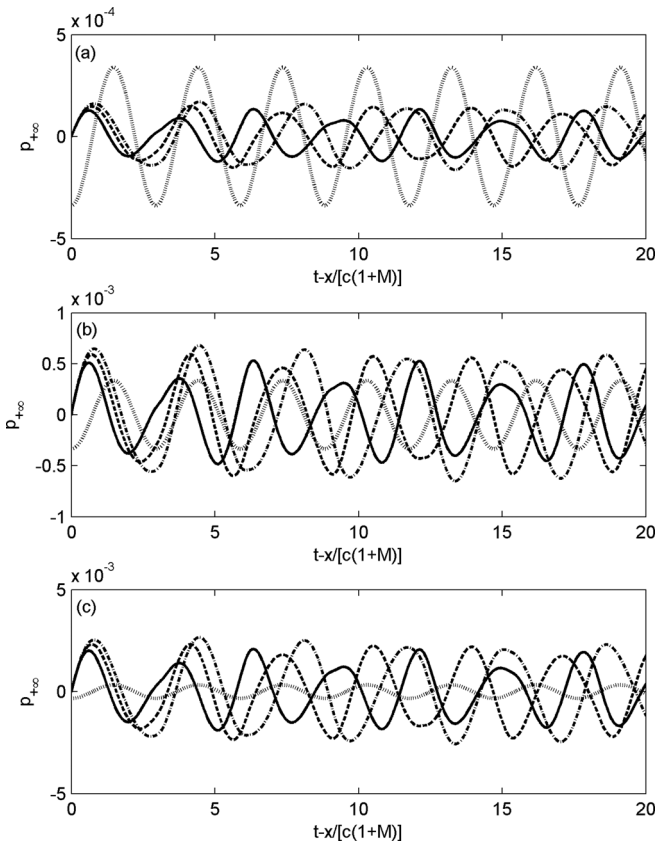

FIG. 7. Effect of mean flow speed and cavity height on the sound radiation of membrane ($\mu_0 = 8, f = 0.34, m = 90, T = 40$). (a) $U = 0.05$, (b) $U = 0.1$, (c) $U = 0.2$. (- - -) p_{dou}, (—) p_{mem} for $h_c = 0.4$, (– – –) p_{mem} for $h_c = 0.6$; (– · –) p_{mem} for $h_c = 0.8$.

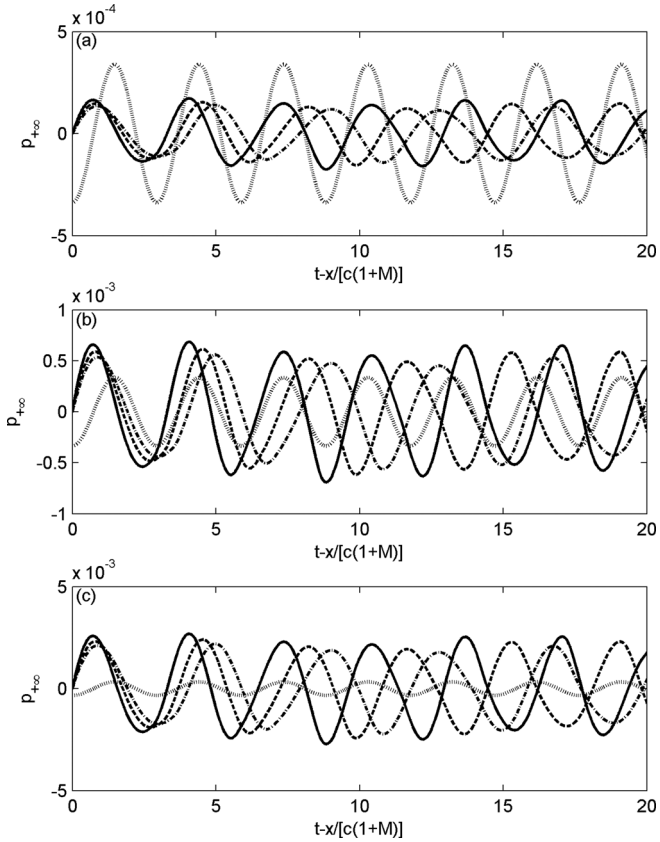

FIG. 8. Effect of mean flow speed and mass ratio on the sound radiation of membrane ($\mu_0 = 8$, $f = 0.34$, $h_c = 0.7$, $T = 40$). (a) $U = 0.05$, (b) $U = 0.1$, (c) $U = 0.2$. (- - -) p_{dou}, (—) p_{mem} for $m = 80$, (– – –) p_{mem} for $m = 100$, (– · –) p_{mem} for $m = 120$.

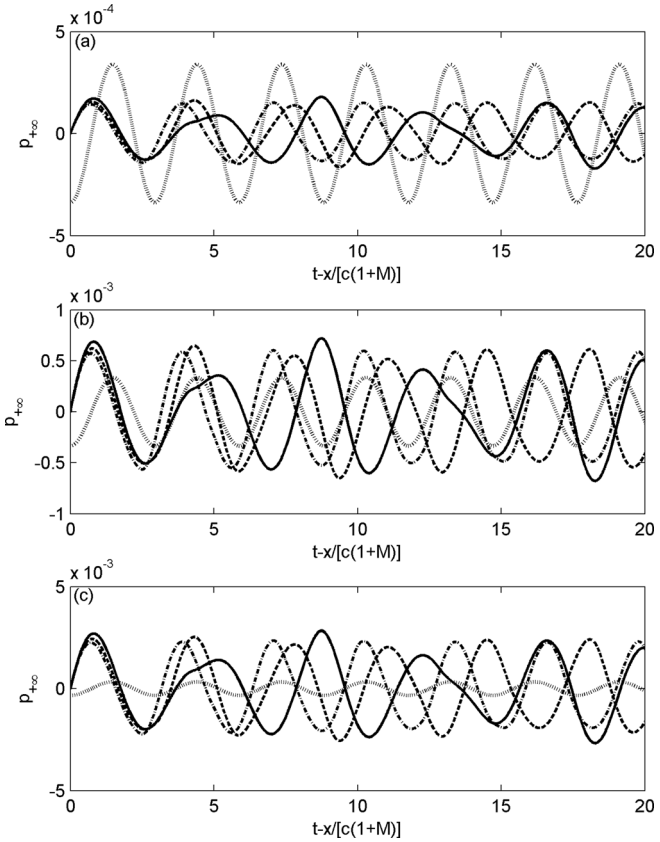

FIG. 9. Effect of mean flow speed and tension on the sound radiation ($\mu_0 = 8$, $f = 0.34$, $h_c = 0.7$, $m = 90$). (a) $U = 0.05$, (b) $U = 0.1$, (c) $U = 0.2$. (- - -) p_{dou}, (—) p_{mem} for $T = 20$, (– – –) p_{mem} for $T = 40$, (– · –) p_{mem} for $T = 60$.

stiffness becomes more significant at lower frequency. Hence, the frequency of sound pressure radiation from the membrane becomes higher for shallower cavity. The same observation could be found for higher mean flow speed, i.e., $U = 0.1$ and 0.2 as illustrated in Figs. 7(b) and 7(c), respectively. From Figs. 7(a) and 7(b), it is observed that, at $\tau \leq 10$, the phase difference between p_{mem} and p_{dou} for $h_c = 0.6$ is small in this period. Therefore, the noise could not be attenuated, but reversely enhanced due to the occurrence of constructive interference. However, if the cavity is replaced by a shallower alternative $h_c = 0.4$, a higher frequency response of the membrane vibration is found. That phase difference between the sound radiated by membrane and doublet in this case is close to $\sim 180°$ at times. As such, a better silencing performance can be achieved and some of the noise from the doublet could be cancelled due to the anti-phase sound radiation of the membrane. Besides the geometric feature of the silencer, the mechanical properties including the mass density and applied tension of the membrane are also regarded as another critical factor to improve the performance of the noise control device. Figure 8 shows the mass effect of the membrane on the sound pressure radiation for cavity height $h_c = 0.7$, $T = 40$, and three different mass ratios, i.e., $m = 80$ (solid line), 100 (dashed line), and 120 (dash-dot line). When the flow speed $U = 0.2$ as shown in Fig. 8(c), the membrane induced sound pressure much higher than that of doublet, i.e., $p_{rms,d}$ is only 17.1% of $p_{rms,m}$ when $m = 120$. The sound radiated by the silencing device is also too large to attenuate the noise from doublet. In Fig. 8, there is a reduction in the amplitude of p_{mem} with the increase of m as a heavier membrane has a greater inertia and hence requires a greater loading to drive a heavier membrane into motion. Figure 8(a) indicates that, when the mass of membrane is reduced from $m = 120$ to 80, the frequency of p_{mem} increases. The same results are obtained if a membrane is used with a higher tension as illustrated by Figs. 9(a) and 9(b). The wave speed c_T, which depends on both the mass ratio and tension of the membrane, becomes high for higher tension or less mass ratio. Therefore, the membrane will oscillate and radiate sound in a higher frequency for higher tension. Figures 9(a) and 9(b) show that the membrane with $T = 60$ radiate sound nearly in the same phase as that of the doublet when the doublet radiates noise at the frequency $f = 0.34$ and strength $\mu_0 = 8$. Thus, two sound waves superimpose together and sum up to induce a larger acoustic pressure. On the other hand, if the tension of membranes is further reduced to $T = 20$ (solid line), the frequency of sound induced by membrane vibration is lower. It is found that the a phase difference comparing between p_{mem} and p_{dou} is close to 180° such that the doublet noise can be canceled by the sound radiated by the membrane and hence the proposed silencing device can only work well at the optimal tension.

Figure 10(a) shows the insertion loss (IL) of the system, expressed as Eq. (13), with different combinations of the

physical properties of membrane, which is represented by c_T. The doublet noise to be controlled with $\mu_0 = 8$ is examined with three different frequency $f = 0.14$, 0.24, and 0.34 which are marked by squares, circles, and crosses, respectively. The cavity depth is kept as constant, i.e., $h_c = 0.7$, and the flow speed is maintained at $U = 0.05$. From the solid and dash-dot line which are marked by square and cross, respectively, only negative IL is obtained when the wave speed of the membrane is ranged from $c_T = 0.471$ to 0.817. It indicated that the performance of the silencing device with such kind of design is poor in attenuating the doublet noise with $f = 0.14$ or 0.34. However, when the noise radiated by the doublet is $f = 0.24$, the silencing device provides positive IL if c_T is smaller than 0.633. The far-field acoustic pressure radiation with $c_T = 0.577$ and 0.471 are illustrated as Figs. 10(b) and 10(c), respectively. Figure 10(b) shows the components of the far-field acoustic pressure induced by the vortex (dotted line), doublet (dashed line), and the membrane vibration (dash-dot line), respectively. The total sound pressure radiation $p_{+\infty}$ by summing up all the components is also indicated by the solid line in Fig. 10(b). The membrane in this case has the properties $m = 120$ and $T = 40$, i.e., $c_T = 0.577$. At the beginning, the amplitude of the total acoustic pressure radiation, $p_{+\infty}$ is close to that of the doublet component p_{dou}. As time passes, $p_{+\infty}$ becomes smaller than p_{dou} since the membrane radiates pressure p_{mem} is anti-

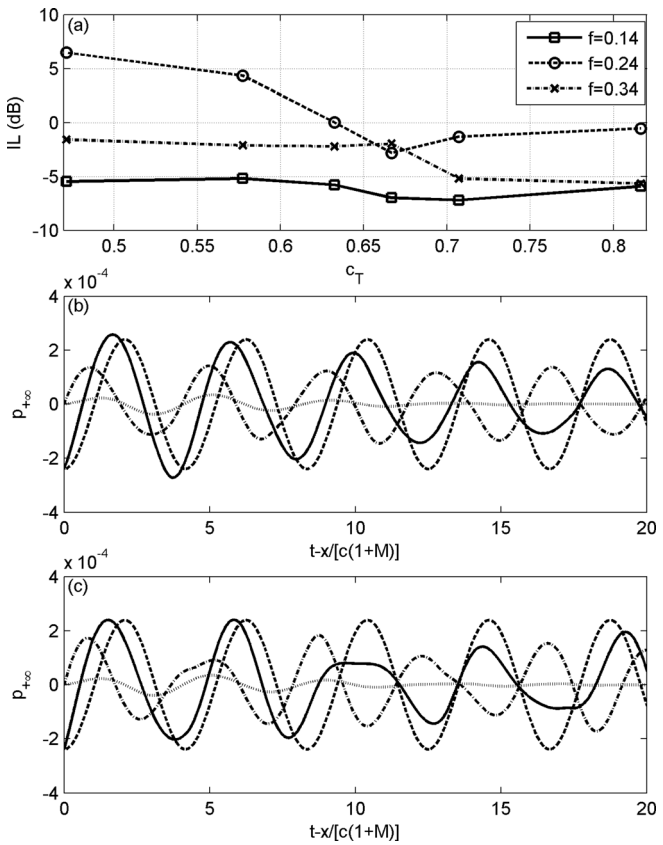

FIG. 10. Silencing performance of proposed membrane housing device. (a) Spectrum of inserting loss (IL). (b) and (c) are the ingredient of sound pressure radiation for $c_T = 0.577$ and $c_T = 0.471$, respectively. (—) total sound pressure radiation, (- - -) pressure radiated by vortex, (– · –) pressure radiated by membrane oscillation, (– – –) pressure radiated by doublet.

phase to p_{dou} such that it cancels part of the doublet noise due to the destructive interference. A similar result can be found in Fig. 10(c) with different physical properties of the membrane. The mass and tension of the membrane is reduced to 90 and 20, respectively, i.e., $c_T = 0.471$, the silencing device suppresses the doublet noise at retarded times larger than 9.4. As shown in Fig. 10(a), the IL for a membrane with $c_T = 0.471$ and $c_T = 0.577$ are 6.483 and 4.339 dB, respectively, in controlling the doublet noise with frequency 0.24. Noise attenuation is achieved from $f = 0.225$ to 0.245 when $c_T = 0.471$. A broader frequency range is covered for the membrane having $c_T = 0.577$, which controls the noise from $f = 0.22$ to 0.245.

IV. CONCLUSIONS

The flow-structure interaction and sound radiation mechanism in the two-dimensional duct system involving doublet and passive noise control devices consisting of flexible boundaries with unsteady flow was investigated in a given time domain in the present study. The time-dependent vortex dynamics and membrane vibration are basically predicted by the adoption of potential theory. The noise attenuation performance of the membrane housing device in controlling the dipole sound radiated from doublet is obtained through the matched asymptotic expansion technique. Several conclusions are drawn.

(1) The motion of the inviscid vortex is strongly associated with the membrane vibration at the corresponding time instant if it is initial shedded at a height which is close to the oscillating membrane, otherwise, the path of the vortex which is dominantly influenced by the doublet shows a significant fluctuating pattern. In addition, the depth of the backed-cavity plays an important role of controlling the motion of the flexible membrane and consequently changing the vortex flight paths.

(2) Amongst the three major sound sources in the duct of the aerodynamic noise generated due to vortex transverse acceleration, the periodic sound radiation from the doublet, and the time varying acoustic pressure by membrane vibration, it is found that the acoustic pressure contribution from the vortex motion in the far field is the least significant. The sound power radiation from the membrane is approximately proportional to mean flow speed with a power of 2. In the very low flow speed range ($0.006 < M < 0.013$), there is slight sound cancellation between the sound radiations from the membrane and doublet in cases of different cavity depths. At the intermediate range of flow speed ($0.013 \leq M \leq 0.018$), the sound radiation from the membrane is strong enough to undergo sound cancellation with the sound waves from the doublet when the cavity depth is appropriately chosen. When the cavity depth is too lengthy, the sound radiation from the membrane would be much higher than noise from the doublet and as a result, imperfect sound cancellation or even more sound radiation to the outlets of the duct would be obtained.

(3) The membrane housing device attenuates the doublet noise based on the sound cancellation mechanism which

strongly depends on the phase difference and the amplitude of sound pressure radiation between the noise source and that radiated by the silencing device. For low frequency noise control, higher mass or lower tension of the membrane can be chosen. For a membrane with tension of 20 and mass ratio of 90 in the cavity of depth 0.7, the proposed membrane housing device can achieve 6 dB insertion loss for controlling the fan with the doublet strength of 8 at a dimensionless frequency of 0.24. Therefore, if the device is designed well with suitable membrane properties and cavity height, good performance of sound attenuation can be achieved.

ACKNOWLEDGMENTS

This project was funded by a General Research Grant from the Hong Kong SAR government (PolyU 5138/12 E) and a studentship from The Hong Kong Polytechnic University.

Beranek, L. L., and Vér, I. L. (**2006**). *Noise and Vibration Control Engineering: Principles and Applications* (Wiley, Hoboken), pp. 279–343.

Brown, C. E., and Michael, W. H. (**1954**). "Effect of leading-edge separation on the lift of a delta wing," J. Aeronaut. Sci. **21**, 690–694.

Choy, Y. S., and Huang, L. (**2002**). "Experimental studies of a drumlike silencer," J. Acoust. Soc. Am. **112**, 2026–2035.

Choy, Y. S., and Huang, L. (**2005**). "Effect of flow on the drumlike silencer," J. Acoust. Soc. Am. **118**, 3077–3085.

Curle, N. (**1955**). "The influence of solid boundaries upon aerodynamic sound," Proc. R. Soc. London, Ser. A **231**, 505–514.

Currie, I. G. (**2013**). *Fundamental Mechanics of Fluids* (CRC, Boca Raton, FL), pp. 73–91.

Dowell, E. H., and Voss, H. M. (**1963**). "The effect of a cavity on panel vibration," AIAA J. **1**, 476–477.

Ffowcs Williams, J. E., and Hawkings, D. L. (**1969**). "Sound generation by turbulence and surfaces in arbitrary motion," Philos. Trans. Roy. Soc. London Ser. A **264**, 321-342.

Frendi, A., Maestrello, L., and Bayliss, A. (**1994**). "Coupling between plate vibration and acoustic radiation," J. Sound Vib. **177**, 207-226.

Fuchs, H. V. (**2001a**). "Alternative fibreless absorbers—New tools and materials for noise control and acoustic comfort," Acta Acust. Acust. **87**, 414–422, available at http://www.ingentaconnect.com/content/dav/aaua/2001/00000087/00000003/art00014.

Fuchs, H. V. (**2001b**). "From advanced acoustic research to novel silencing procedures and innovative sound treatments," Acta Acust. Acust. **87**, 407–413, available at http://www.ingentaconnect.com/content/dav/aaua/2001/00000087/00000003/art00013.

Gutin, L. (**1948**). "On the sound field of a rotating propeller," NACA TM No. **1195**, 1–21, available at https://ntrs.nasa.gov/search.jsp?R=20030068996.

Howe, M. S. (**1998**). *Acoustics of Fluid-Structure Interactions* (Cambridge University Press, Cambridge), pp. 27–33.

Howe, M. S. (**2003**). *Theory of Vortex Sound* (Cambridge University Press, New York), pp. 25–40.

Huang, L. (**1999**). "A theoretical study of duct noise control by flexible panels," J. Acoust. Soc. Am. **106**, 1801–1809.

Huang, L. (**2002**). "Modal analysis of a drumlike silencer," J. Acoust. Soc. Am. **112**, 2014–2025.

Huang, L., Choy, Y. S., So, R. M. C., and Chong, T. L. (**2000**). "Experimental study of sound propagation in a flexible duct," J. Acoust. Soc. Am. **108**, 624–631.

Ingard, K. U. (**1995**). *Notes on Sound Adsorption Technology* (Noise Control Foundation, Poughkeepsie, NY), Chap. 3, pp. 1–18.

Ji, Z. L. (**2005**). "Acoustic attenuation performance analysis of multi-chamber reactive silencers," J. Sound Vib. **283**, 459–466.

Katz, J., and Plotkin, A. (**2001**). *Low Speed Aerodynamics* (Cambridge University Press, Cambridge), pp. 17–20.

Kim, H. S., Kim, S. R., Lee, S. H., Seo, Y. H., and Ma, P. S. (**2016**). "Sound transmission loss of double plates with an air cavity between them in a rigid duct," J. Acoust. Soc. Am. **139**, 2324–2333.

Kowalczyk, K., and Van Walstijn, M. (**2008**). "Formulation of locally reacting surfaces in FDTD/K-DWM modelling of acoustic spaces," Acta Acust. Acust. **94**, 891–906.

Lighthill, M. J. (**1952**). "On sound generated aerodynamically. I. General theory," Proc. R. Soc. London, Ser. A **211**, 564–587.

Liu, Y., Choy, Y. S., Huang, L., and Cheng, L. (**2012**). "Noise suppression of a dipole source by tensioned membrane with side-branch cavities," J. Acoust. Soc. Am. **132**, 1392–1402.

Liu, Y., Choy, Y. S., Huang, L., and Cheng, L. (**2014**). "Reactive control of subsonic axial fan noise in a duct," J. Acoust. Soc. Am. **136**, 1619–1630.

Longhouse, R. (**1977**). "Vortex shedding noise of low tip speed, axial flow fans," J. Sound Vib. **53**, 25–46.

Munjal, M. L. (**1987**). *Acoustics of Ducts and Mufflers: With Application to Exhaust and Ventilation System Design* (Wiley, New York), pp. 42–103.

Ostoich, C. M., Bodony, D. J., and Geubelle, P. H. (**2013**). "Interaction of a Mach 2.25 turbulent boundary layer with a fluttering panel using direct numerical simulation," Phys. Fluids **25**, 110806.

Peake, N. (**2004**). "On the unsteady motion of a long fluid-loaded elastic plate with mean flow," J. Fluid Mech. **507**, 335–366.

Sabina, F. J., and Babich, V. M. (**2001**). "Low-frequency scattering of acoustic waves by a bounded rough surface in a half-plane," J. Acoust. Soc. Am. **109**, 878–885.

Sabina, F. J., and Willis, J. R. (**1975**). "Scattering of SH waves by a rough half-space of arbitrary slope," Geophys. J. R. Astron. Soc. **42**, 685–703.

Saffman, P. G. (**1992**). *Vortex Dynamics* (Cambridge University Press, Cambridge), pp. 95–115.

Sharland, I. (**1964**). "Sources of noise in axial flow fans," J. Sound Vib. **1**, 302–322.

Sucheendran, M. M., Bodony, D. J., and Geubelle, P. H. (**2013**). "Coupled structural-acoustic response of a duct-mounted elastic plate with grazing flow," AIAA J. **52**, 178–194.

Taflove, A., and Brodwin, M. E. (**1975**). "Numerical solution of steady-state electromagnetic scattering problems using the time-dependent Maxwell's equations," IEEE Trans. Microwave Theory Tech. **23**, 623–630.

Tang, S. K. (**2011**). "Vortex sound in the presence of a low Mach number flow across a drum-like silencer," J. Acoust. Soc. Am. **129**, 2830–2840.

Tang, S. K., Leung, R. C. K., So, R. M. C., and Lam, K. M. (**2005**). "Acoustic radiation by vortex induced flexible wall vibration," J. Acoust. Soc. Am. **118**, 2182–2189.

Vallentine, H. R. (**1959**). *Applied Hydrodynamics* (Butterworths Scientific Publications, London), pp. 102–135.

Wang, J., Huang, L., and Cheng, L. (**2005**). "A study of active tonal noise control for a small axial flow fan," J. Acoust. Soc. Am. **117**, 734–743.

Zhang, Q., and Bodony, D. J. (**2016**). "Numerical investigation of a honeycomb liner grazed by laminar and turbulent boundary layers," J. Fluid Mech. **792**, 936–980.